

Supporting Information

Operando pH Measurements Decipher H⁺/Zn²⁺

Intercalation Chemistry in High-Performance

Aqueous Zn/ δ -V₂O₅ Batteries

Xu Liu,^{1,2} Holger Euchner,¹ Maider Zarrabeitia,^{1,2,3} Xinpei Gao,^{1,2} Giuseppe Antonio

Elia,^{1,2} Axel Groß,^{1,4} Stefano Passerini^{1,2*}*

¹ Helmholtz Institute Ulm (HIU), Helmholtzstrasse 11, D-89081 Ulm, Germany

² Karlsruhe Institute of Technology (KIT), P.O. Box 3640, D-76021 Karlsruhe, Germany

³ Centre for Cooperative Research on Alternative Energies (CIC energiGUNE), Basque

Research and Technology Alliance (BRTA), Alava Technology Park, Albert Einstein 48,

01510 Vitoria-Gasteiz, Spain

⁴ University of Ulm, Institute of Theoretical Chemistry, Albert-Einstein-Allee 11, D-89081

Ulm, Germany

Corresponding Authors

*E-mail: giuseppe.elia@kit.edu; stefano.passerini@kit.edu

Experimental details

1. Materials

Ca(CH₃COO)₂ (99%, Sigma Aldrich), V₂O₅ (Pechiney), *N*-Methyl-2-pyrrolidone (NMP, anhydrous, Sigma Aldrich), NaOH (99%, Alfa Aeara), polyvinylidene fluoride (PVdF, Solef 6020), carbon black (Super C65, IMERYS), stainless steel foil (thickness: 50 μm, Goodfellow), zinc foil (thickness: 25 μm, Goodfellow), activated carbon (AC, YP-47, Kuraray), polytetrafluoroethylene dispersion (60 wt.% in water, Sigma Aldrich), carbon paper (TP-030T, Quintech), glass fiber sheet (Whatman GF/F), sulphuric acid (98%, Merck), and SiO₂ aerogel powder (Sigma Aldrich) were used as received. The pH buffer solutions were purchased from SI Analytics GmbH and directly used. For aqueous solution, Zn(CF₃SO₃)₂ (99.5%, 50 ppm water, Solvionic) was directly used, while for nonaqueous electrolytes, it was dried at 120 °C under vacuum (10⁻³ mbar) for 12 h before use. Molecular sieves (3 Å, Alfa Aesar) were dried at 300 °C under vacuum (10⁻³ mbar) for more than one week. Acetonitrile (ACN, VWR, anhydrous) was dried with the molecular sieves to remove the residual water before being used for the electrolyte preparation. GO was prepared according to a modified Hummers' method.¹

2. Preparation of CVO/rGO composites

A stirring bar, 1 mmol Ca(CH₃COO)₂, 2 mmol V₂O₅ powder, and 20 mL 0.9 g/L GO aqueous dispersion were mixed in a glass reactor (30 mL, from Anton Paar company). Then, the suspension was heated in a "Monowave 300" microwave oven (Anton Paar) using the "Heat as fast as possible" mode at 180 °C for 2 h with a stirring rate of 300 rpm. The obtained product was centrifuged, and the greenish precipitate was thoroughly washed with water and acetone. After evaporation of the residual acetone in an oven with a temperature of 80 °C, the final CVO/rGO powder was obtained.

3. Characterization

X-ray diffraction (XRD) was conducted using a Bruker D8 Advance diffractometer (Bruker, Germany) with Cu-Kα radiation. The calcium and vanadium content in the composite

was determined by inductively coupled plasma - optical emission spectrometry (ICP-OES) carried out on a Spectro Arcos spectrometer (Spectro Analytical Instruments). Scanning electron microscope (SEM) investigation of materials and electrodes was performed with a Zeiss LEO 1550 microscope equipped with an EDS spectrometer (Oxford Instruments X-MaxN, 50 mm², 15kV). Raman spectra were recorded with Renishaw 2000 equipped with a He-Ne laser (633 nm). Thermogravimetric analysis (TGA) was carried out on TA Q2000 apparatus heating the powder up to 400 °C with a heating rate of 5 °C min⁻¹ under oxygen flow. X-ray photoelectron spectroscopy (XPS) measurements were conducted in an ultrahigh vacuum surface analysis system (10⁻¹⁰ mbar) by Phoibos 150 XPS spectrometer (SPECS –Surface concept) equipped with a micro-channel plate and Delay Line Detector (DLD) and monochromatized Al K α (1486.6 eV) X-ray. The peak fitting was carried out by CasaXPS software.

4. Cell assembly and electrochemical measurements

The CVO/rGO electrodes were fabricated by doctor-blade casting of slurries with 70 wt. % active materials, 20 wt. % C65, and 10 wt. % PVdF on stainless steel/carbon paper substrates. The electrodes with carbon paper substrate were only used for *operando* pH measurements. NMP was used as the solvent for the slurry. After drying at 60 °C, electrodes with a diameter of 12 mm were punched and further dried at 120 °C under high vacuum to fully remove the NMP. The average mass loading of the active material was around 2 mg cm⁻². The specific capacity is calculated based on the mass of CVO/rGO composite. Freestanding AC electrodes were fabricated according to the procedure reported before.² The mass ratio of AC active material to PTFE binder is 8:2.

For coin cell type AZMBs, zinc foil disc with a diameter of 16 mm, GF/F glass fiber disc with a diameter of 16 mm, and 100 μ L 3 m Zn(OTF)₂ aqueous solutions were used as the counter electrodes, separators, electrolytes, respectively. To enhance the cyclability of the zinc electrodes, 10 wt.% SiO₂ aerogel powder was added to the electrolytes.³ For three-electrode

Swagelok type AZMBs, zinc foil discs with a diameter of 12 mm and around 2 mm were used as the counter and reference electrodes, respectively. GF/F membrane discs and 100 μ L 3 m Zn(OTF)₂ aqueous solutions were used as separators and electrolytes, respectively. Three electrode Swagelok type T cells were assembled to investigate the electrochemical behavior of CVO/rGO in nonaqueous electrolytes. Zinc foil discs with a diameter of 12 mm and around 2 mm were used as the counter and reference electrodes, respectively. GF/F membrane discs and 100 μ L 1 M Zn(OTF)₂-ACN solutions were used as separators and electrolytes, respectively. Three-electrode Swagelok type T cells were designed to investigate the proton intercalation behavior in CVO/rGO. The scheme of the cell configuration for *operando* pH measurements is shown in Figure 3a. The pH electrode with a flat membrane was purchased from WTW-XYLEM (Blue line 27 pH, WTW-pH surface measurement with SenTix® Sur).⁴

A Maccor 4000 Battery system (Maccor, USA) was used for the galvanostatic charge/discharge tests. Cyclic voltammetry tests were carried out with a galvanostat/potentiostat (VMP3 Bio-Logic, France). Galvanostatic intermittent titration technique (GITT) was performed with the Maccor 4000 Battery system on three electrodes Swagelok type AZMBs (10 mA g⁻¹ for 2 h followed by a 16 h rest). For *operando* pH measurement, the charge/discharge of the cell was controlled via a galvanostat/potentiostat VMP (Bio-Logic, France) while the pH values were recorded every 5 minutes via a pH meter (Lab 860, SI Analytics).

Computational details

1. DFT Calculations

Density functional theory (DFT) calculations were conducted with the periodic plane wave code VASP (Vienna ab initio simulation package).⁵ Within the VASP code, the electron-ion interaction is adequately described by the pseudopotential approach, which was applied in the generalized form of the projector augmented wave method.⁶ For this work, spin-polarized calculations were performed, and the generalized gradient approximation in the formulation of

Perdew, Burke, and Ernzerhof (PBE) was applied to account for exchange and correlation.⁷

The starting point for the computational study was the structure of $\delta\text{-V}_2\text{O}_5\cdot\text{H}_2\text{O}$ phase, because, as discussed in the main text Ca ions were removed upon the first charge. In a first simplified approach, the structural water were removed and the remaining V_2O_5 layer structure, consisting of 28 atoms in the unit cell, was optimized with respect to lattice parameter and atomic positions, using an energy cutoff of 600 eV and a $3\times 9\times 3$ Γ -centered k-point mesh. In subsequent calculations, different numbers of H and Zn atoms were inserted in between the layers of the structure, allowing for the investigation of the respective intercalation process. The energetically most stable structures that were obtained by DFT for the respective Zn and hydrogen contents are depicted in Figure S12.

In the next step, structural water was included in the calculations, and a model structure, corresponding to $\delta\text{-V}_2\text{O}_5\cdot\text{H}_2\text{O}$ was constructed, now consisting of 40 atoms per unit cell. The main impact of the structural water is an increasing layer distance, while the layer structure remains intact. Different configurations with Zn and hydrogen intercalated were investigated. The energetically most stable structures that could be identified from our DFT calculations are shown in Figure S13.

2. Phase diagrams

The stability of the intercalation compounds with respect to temperature and pressure is determined by Gibb's free energy differences with respect to the empty V_2O_5 framework and the intercalating species. The H/Zn reservoir in the electrolyte is described in a grand-canonical approach in the spirit of the computational hydrogen electrode (CHE).⁸ In analogy to the Gibb's free energy of adsorption, which is typically used in surface science, we define the Gibb's free energy of insertion as:

$$\Delta G = G(H_{n_H} Zn_{n_{Zn}} V_2 O_5) - G(V_2 O_5) - \sum_i n_i \mu_i$$

In our case, G represents the Gibb's free energy of the V_2O_5 compound and the different

intercalation compounds. The μ_i are the chemical potentials of hydrogen and Zn in solution, while n_i is the number of hydrogen and Zn atoms that are inserted in the host matrix. Since the species that are to be inserted originate from charged ions in solution, we actually have to consider the so-called electrochemical potential

$$\tilde{\mu}_i = \mu_i + z_i e U,$$

with U the potential of the electrode, z_i the charge of the particle and e the elementary charge. Within the concept of the CHE, the explicit calculation of solvation energies is avoided. This concept makes use of the fact that at standard conditions, which define the standard hydrogen potential (U_{SHE}), hydrogen in the gas phase and protons in solution are in equilibrium. Furthermore, it is well-known how the electrochemical potential of solvated protons changes with electrode potential and pH. Thus one arrives at the following expression:

$$\tilde{\mu}_{H^+}(aq) + \tilde{\mu}_{e^-} = \frac{1}{2}\mu_{H_2}(g) - eU_{SHE} - k_B T \ln(10) pH$$

This concept can be extended to any other redox couple such that for the solvated Zn ions we can analogously write:

$$\tilde{\mu}_{Zn^{2+}}(aq) + 2\tilde{\mu}_{e^-} = \mu_{Zn}(bulk) - 2e(U_{SHE} - U^0) - k_B T \ln a_{Zn^{2+}}$$

The standard potential U^0 of Zn/Zn²⁺ vs. the standard hydrogen electrode is -0.76 V, and $a_{Zn^{2+}}$ denotes the activity of Zn in solution being.

By subtracting the total energy of the hydrogen gas and bulk Zn we can normalize the electrochemical potential, thus obtaining:

$$\Delta\tilde{\mu}_H = \tilde{\mu}_{H^+}(aq) + \tilde{\mu}_{e^-} - \frac{1}{2}E_{H_2} = -eU_{SHE} - k_B T \ln(10) pH$$

$$\Delta\tilde{\mu}_{Zn} = \tilde{\mu}_{Zn^{2+}}(aq) + 2\tilde{\mu}_{e^-} - E_{Zn} = -2e(U_{SHE} - U^0) - k_B T \ln a_{Zn^{2+}}$$

By incorporating these terms in the Gibb's free energy of insertion we finally obtain the

following expression:

$$\Delta G = \Delta E_f - \sum_i n_i \Delta \tilde{\mu}_i(T, c_i, U)$$

Here ΔE_f denotes the energy of formation as obtained from our above described DFT calculations:

$$\Delta E_f = E(H_{n_H}Zn_{n_{Zn}}V_2O_5) - E(V_2O_5) - n_{Zn}E(Zn) - \frac{1}{2}n_H E(H_2)$$

with $E(H_{n_H}Zn_{n_{Zn}}V_2O_5)$ and $E(V_2O_5)$ the DFT total energies for the intercalated/deintercalated vanadium oxide compounds and $E(Zn)$ and $\frac{1}{2}E(H_2)$ the total energies of bulk Zn and hydrogen gas. In this last step, we have replaced the Gibbs free energies of the bulk phases by the total energies that can directly be obtained from DFT calculations. This step is based on the assumption that the dependence of the free energy of the bulk phases on temperature and the presence of the electrochemical environment can be neglected.⁹

Evaluating this formula for the different configurations allows to construct the corresponding phase diagram as a function of the electrochemical potential and thus of the pH value (see main text).

Reference:

- (1) Marcano, D. C.; Kosynkin, D. V.; Berlin, J. M.; Sinitiskii, A.; Sun, Z. Z.; Slesarev, A.; Alemany, L. B.; Lu, W.; Tour, J. M. Improved Synthesis of Graphene Oxide. *ACS Nano* 2010, 4, 4806–4814.
- (2) Leyva-García, S.; Lozano-Castelló, D.; Morallón, E.; Vogl, T.; Schütter, C.; Passerini, S.; Balducci, A.; Cazorla-Amorós, D. Electrochemical Performance of A Superporous Activated Carbon in Ionic Liquid-Based Electrolytes, *Journal of Power Sources*, 2016; 333, 419-426.
- (3) Chao, D. L.; Zhu, C. R.; Song, M.; Liang, P.; Zhang, X.; Tiep, N. H.; Zhao, H. F.; Wang, J.; Wang, R. M.; Zhang, H.; Fan, H. J. A High-Rate and Stable Quasi-Solid-State Zinc-Ion

Battery with Novel 2D Layered Zinc Orthovanadate Array. *Advanced Materials*, 2018, 1803181.

(4)<https://www.xylemanalytics.com/en/general-product/id-39/WTW---pH-surface-measurement-with-SenTix®-Sur>

(5) Kresse, G. and Furthmüller, J. Efficient iterative schemes for ab initio total-energy calculations using a plane-wave basis set. *Phys. Rev. B* 54, 11169–11186 (1996).

(6) Kresse, G. and Joubert, D. From ultrasoft pseudopotentials to the projector augmented-wave method. *Phys. Rev. B* 59, 1758–1775 (1999).

(7) Perdew, J. P., Burke, K. & Ernzerhof, M. Generalized Gradient Approximation Made Simple. *Phys. Rev. Lett.* 77, 3865–3868 (1996).

(8) Peterson A. A., Abild-Pedersen F., Studt, F., Rossmeisl J. and Norskov, J. K., *Energy Environ. Sci.* 3, 1311 (2010)

(9) Reuter K. and Scheffler M., *Phys. Rev. B* 65, 035406 (2001)).

Supplementary Note 1

Comparing the CV curves (Fig. 1c) and the evolution of pH versus voltage (Fig. 3c), one can correlate the contribution of H^+ or Zn^{2+} intercalation chemistry with the multiple CV peaks. However, a clear assignment of these CV peaks to specific intercalated species still faces two main difficulties.

The first one is that the contribution of Zn^{2+} intercalation/release in the regions where the pH varies is still not clear. For example, it is clear that H^+ contributes to Peak 5 in the first cycle, but whether Zn^{2+} intercalation also occurs is still unknown.

The second difficulty is that the CV peaks are very broad and overlapping. In the regions where pH variation trend changes, it is difficult to assign the CV peak to a specific carrier. For example, in the charging process, the pH is nearly stable between 0.9 and 1.0 V (an indication of Zn^{2+} de-intercalation), but decreases between 1.0 and 1.2 V (an indication of H^+ de-intercalation). However, the CV curves exhibit only one peak (Peak 8) in the 0.9-1.2 V interval, particularly in the second and third cycles.

Supplementary Note 2

The interaction between the intercalated cations and the V-O layers depends on the charge density of the cation. When H_2SO_4 aqueous solution is employed as the electrolyte, water molecules co-intercalate with the protons, effectively decreasing their charge density. While in the nonaqueous $Zn(OTF)_2/ACN$ electrolyte, desolvated divalent Zn^{2+} with higher charge density respect to solvated protons is intercalated into the CVO. Therefore, the interlayer distance of Zn^{2+} -intercalated CVO is even lower than that of H^+ -intercalated CVO.

Supplementary Note 3

The intercalation behavior of the CVO highly depends on the employed electrolyte.

As mentioned above, in aqueous electrolytes, water molecules can be incorporated into the interlayer and decrease the charge density of the intercalated ions, e.g., H^+ as well as Zn^{2+} , mitigating the lattice breath. Thus, the decrease of the interlayer distance observed in

nonaqueous $\text{Zn}(\text{OTF})_2/\text{ACN}$ cannot be directly related to that of the $\text{Zn}(\text{OTF})_2/\text{H}_2\text{O}$ electrolyte.

In 0.01 M H_2SO_4 aqueous electrolyte, H^+ is the only cation that can interact with CVO. But in 3 m $\text{Zn}(\text{OTF})_2$ aqueous electrolyte, both H^+ and Zn^{2+} can be intercalated, actually being in competition. Due to this inherent difference, the observed H^+ intercalation in CVO in 0.01 M H_2SO_4 aqueous electrolyte does not grant its occurrence in 3 m $\text{Zn}(\text{OTF})_2$ aqueous electrolyte, even in the same potential region.

In addition, the different electrolyte ionic conductivities also influence the electrochemical behavior of the CVO.

Supplementary Note 4

Since the same electrode material and electrolyte, i.e., CVO/rGO, zinc foil, and 3 m $\text{Zn}(\text{OTF})_2$ aqueous solution, were used in the coin cells and the operando pH cells, the different reversibility may only originate from the different cell configuration, e.g., the current collectors and the internal pressure. The electronic transport in the sandwich-type current collector, i.e., stainless steel strip-carbon paper-CVO electrode, relies on a tight, intimate contact, which could be affected by the insufficient internal pressure as there is no spring in the *operando* pH cell. In fact, the glass-made, sensitive pH electrode does not allow the high pressure as in the coin cell.

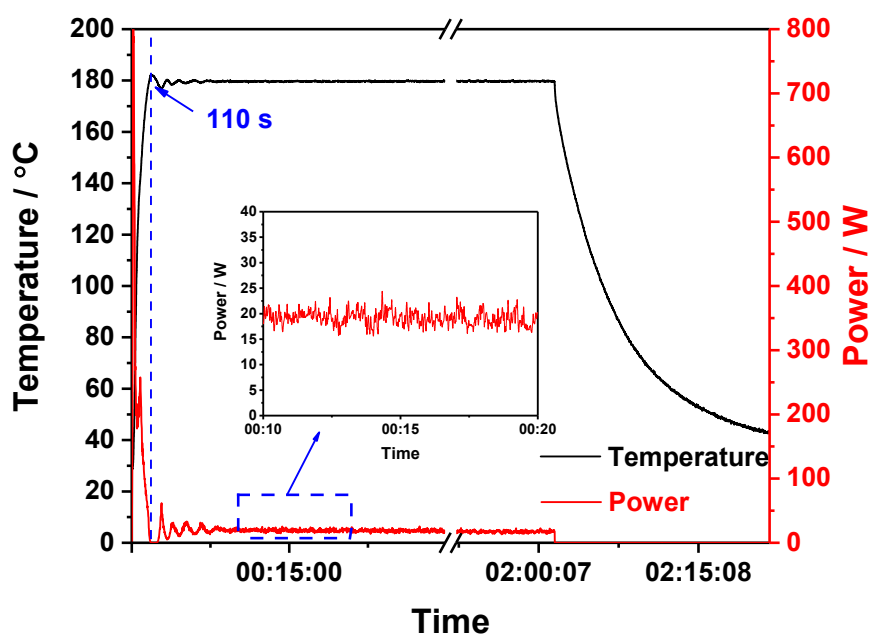


Fig. S1. Evolution of temperature and power during the microwave reaction to CVO/rGO. The data was directly recorded by the microwave reactor. The inset shows the power needed to keep the temperature constant during 10-20 minutes.

Only 110 s were required to reach 180 °C, after which a power as low as 20 W was sufficient to keep the temperature constant.

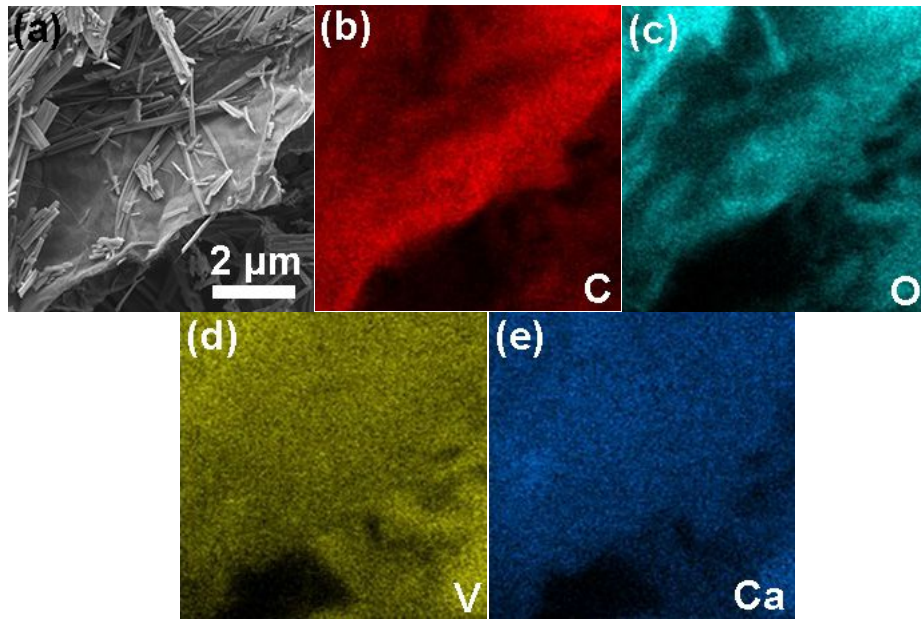


Fig. S2. (a) SEM image of as-prepared CVO/rGO composite and corresponding distribution of (b) C, (c) O, (d) V, and (e) Ca measured via EDS.

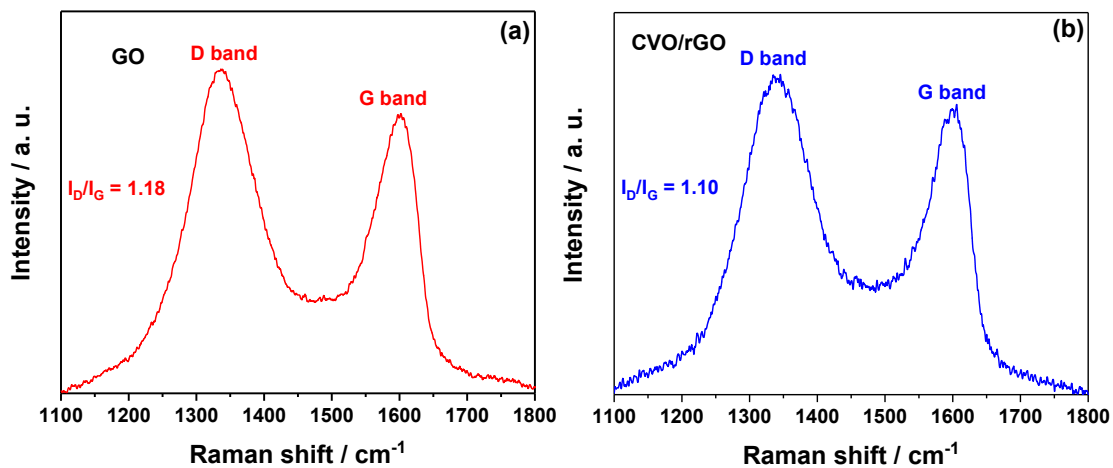


Fig. S3. Raman spectra of (a) the GO powder and (b) the CVO/rGO.

The intensity ratio of the D and G bands (at 1335 and 1600 cm⁻¹) of CVO/rGO is 1.10 which is slightly lower than that of the GO (1.18). Therefore, GO is partially reduced during the microwave-assisted hydrothermal synthesis.

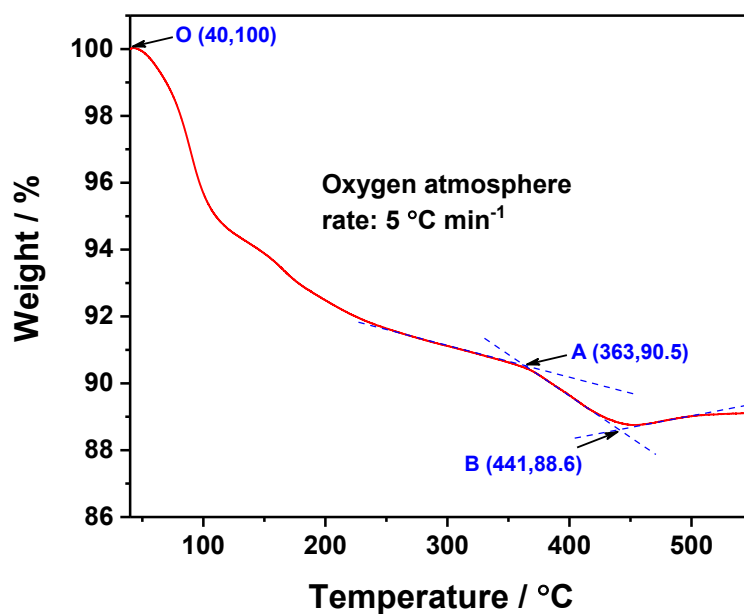


Fig. S4. TGA curve of as-prepared CVO/rGO composite in oxygen atmosphere with a heating rate of 5 °C min⁻¹.

From 40 to 363 °C, the weight loss (around 9.5 wt. %) can be attributed to the absorbed water and structural water. The weight loss (1.9 wt. %) between 363 and 441 °C can be assigned to the rGO in the composite. With a temperature higher than 441 °C, the V⁴⁺ in CVO starts to be oxidized, which thereafter leads to an increase of the weight.

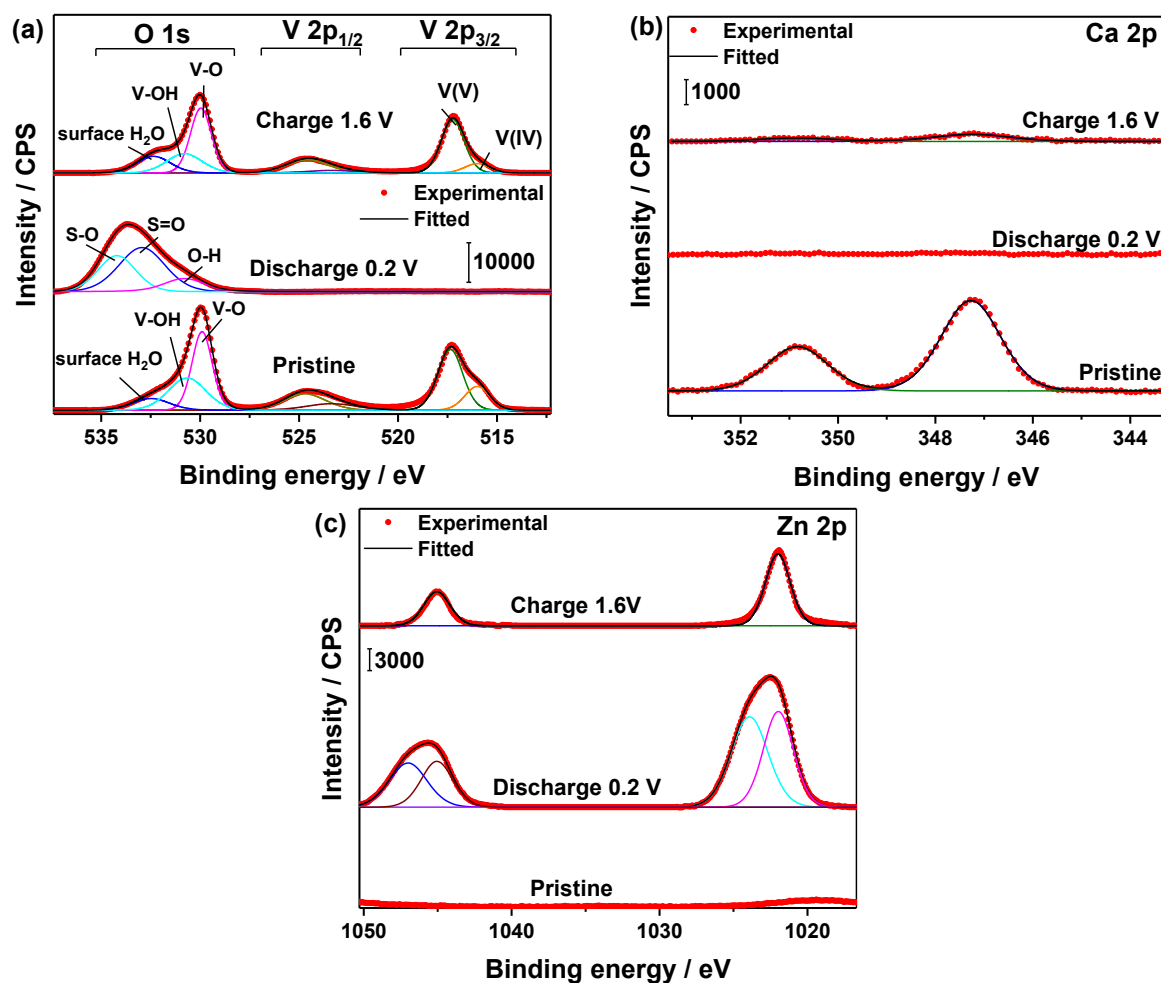


Fig. S5. XPS spectra of pristine, fully discharged, and fully charged CVO/rGO electrodes: (a) O 1s and V2p, (b) Ca 2p, and (c) Zn 2p core-level. 3 m Zn(OTF)₂ aqueous electrolyte.

For the fully discharged electrode, the signal of V 2p and Ca 2p cannot be detected. Meanwhile the O 1s and Zn 2p peaks exhibit significant shift compared with that of the pristine electrode. As evidenced via XRD (Fig. 2a) and SEM (Fig. S8), Zn₁₂(CF₃SO₃)₉(OH)₁₅·xH₂O formed during the discharge process covers the surface of

the electrode. The peaks located at 530.80, 532.95, and 534.21 eV, in the O 1s spectrum at discharged state, can be indexed to OH, S=O, and S-O, respectively. The first one originates from the OH⁻, while the rest two result from the OTF⁻. Obviously, the Zn²⁺ in this additional compound has two different chemical environments, of which the origin is not known, but is not relevant for the present study.

When the electrode is charged back to 1.6 V, the V 2p appears again, and the O 1s shows the same shape as the initial state despite more surface water is observed compared with the pristine electrode. This demonstrates that the additional phase covering the electrode surface disappears upon charge, which matches well with the XRD (Fig. 2a) and SEM (Fig. S8) results. Also, the intensity of Ca 2p after charge remains rather low, once more supporting for the irreversible Ca²⁺ de-intercalation. The occurrence of the Zn 2p signal in the pattern of the fully charged electrode can be attributed to Zn₃(OH)₂V₂O₇·3H₂O formed during the charging process.

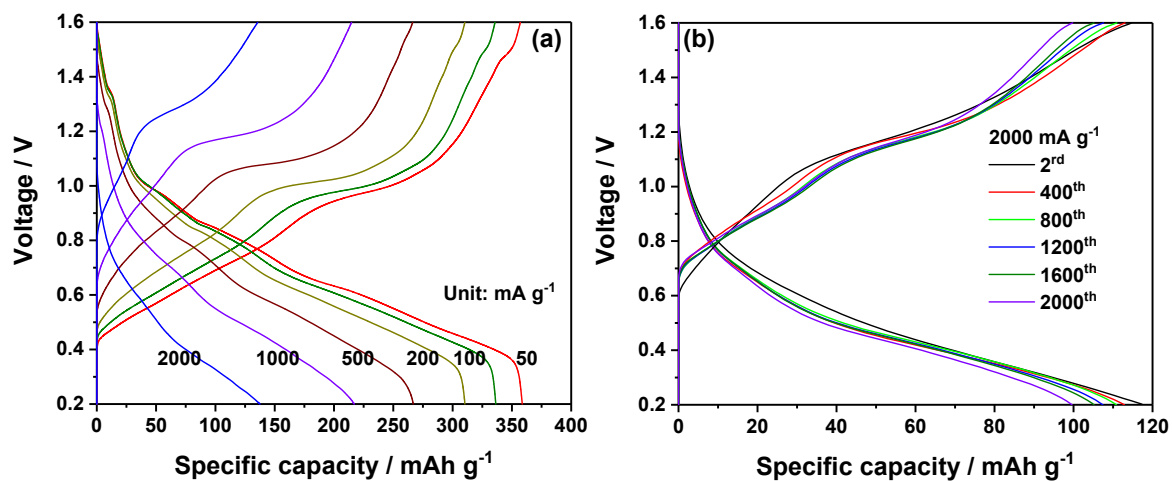


Fig. S6. Charge-discharge profiles of Zn//CVO/rGO AZMB at (a) various specific currents and (b) selected cycles upon cycling at a specific current of 2000 mA g⁻¹. Coin cell, 3 m Zn(OTF)₂ aqueous electrolyte.

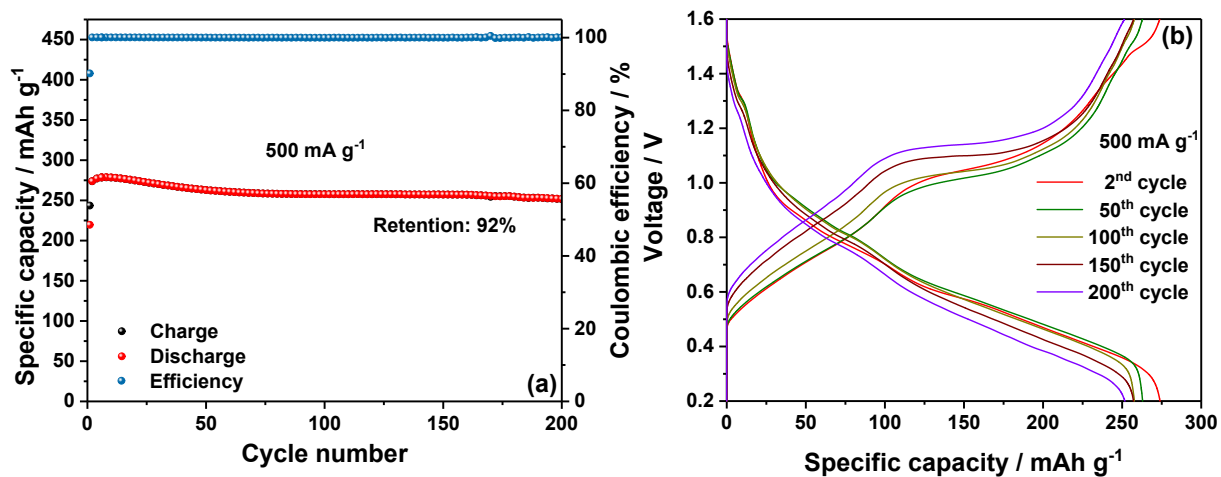


Fig. S7. (a) Specific capacity and Coulombic efficiency and (b) charge-discharge

profiles at the selected cycles of the CVO/rGO electrode in an AZMB cell upon cycling

at 500 mA g⁻¹. Coin cell, 3 m Zn(OTF)₂ aqueous electrolyte.

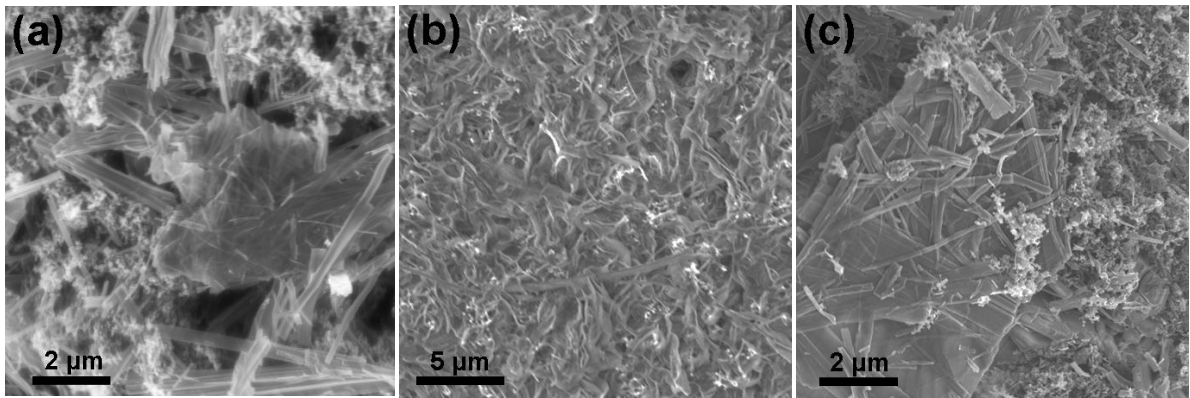


Fig. S8. The SEM images of (a) pristine, (b) fully discharged and (c) fully charged CVO/rGO electrodes disassembled and washed in air atmosphere. Electrolyte: 3 m Zn(OTF)₂ aqueous electrolyte.

In both the pristine and fully charged electrodes, the typical morphology of the CVO/rGO can be observed (Fig. S8 a and c). But the surface of the fully discharged electrode is covered with a dense layer. Correlating the results from XRD (Fig. 2a) and XPS (Fig. S5), one can conclude that this layer is the formed $\text{Zn}_{12}(\text{CF}_3\text{SO}_3)_9(\text{OH})_{15}\cdot x\text{H}_2\text{O}$ observed in the XRD patterns of the deep discharged samples.

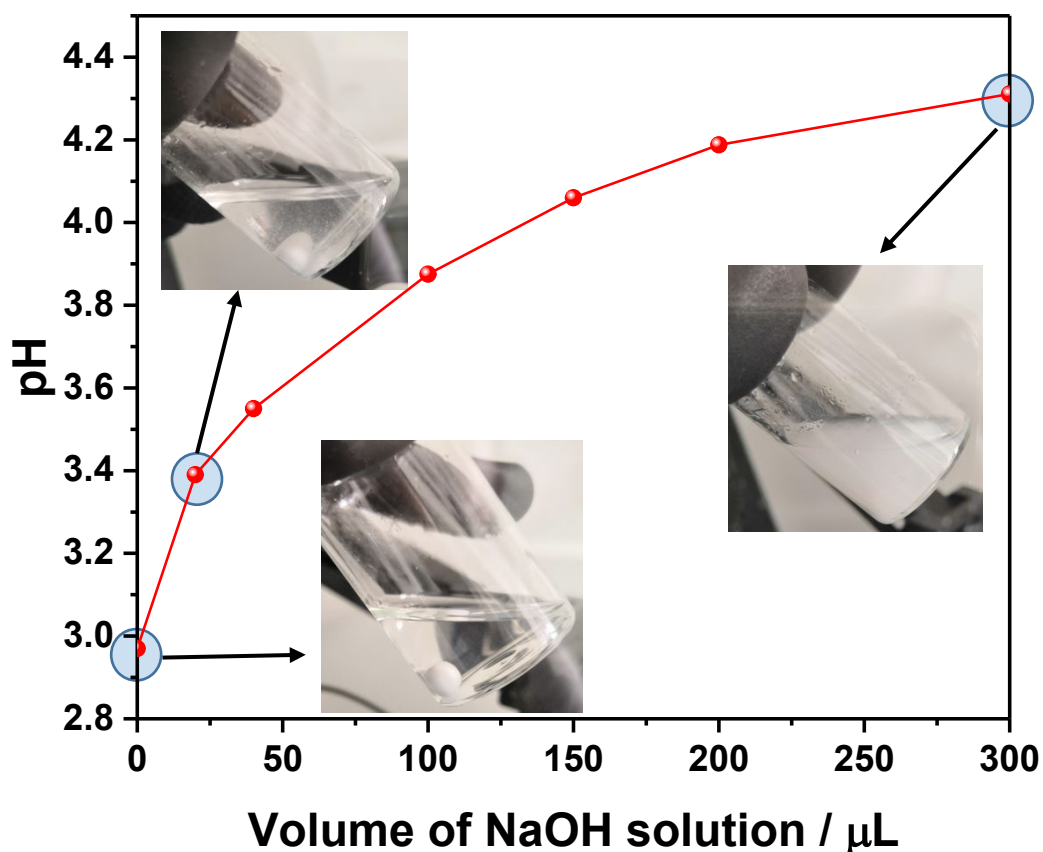


Fig. S9. pH evolution upon titration of 4.18 mL 3 m $\text{Zn}(\text{OTF})_2$ aqueous solution with 3.26 M NaOH aqueous solution. The insets show the pictures of the solution upon the titration.

To mitigate the influence of CO_2 in air, the titration was performed in a glove box flushed with Ar. MilliQ water was degassed bubbling N_2 for 1 h before being used to prepare the solution. The pH evolution upon titration is displayed as follows. The initial pH of the 3 m $\text{Zn}(\text{OTF})_2$ aqueous solution is 2.970. With 20 μL 3.26 M NaOH solution added, the pH increases to 3.39, at which some white precipitates can be observed. For a further addition of NaOH, i.e., pH increase, the white precipitate amount increases. Therefore, the formation of the BZS is clearly susceptible to the pH variation.

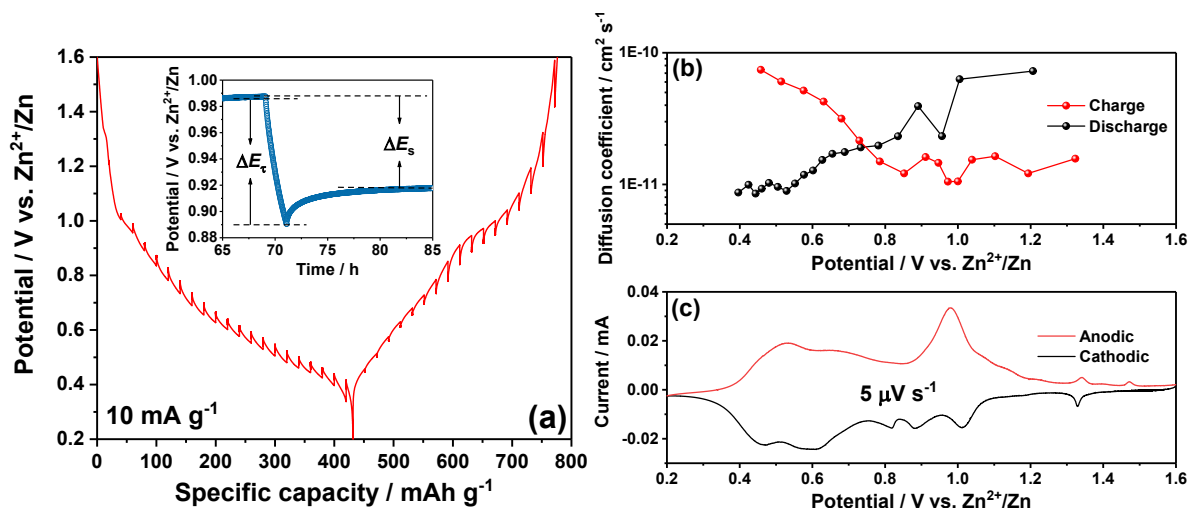


Fig. S10. (a) GITT curves of the CVO/rGO electrode in three-electrode Swagelok-type AZMBs (each step corresponds to a current flow of 10 mA g^{-1} for 2 h followed by 16 h rest). The inset displays a typical potential-time profile during the GITT measurement. (b) Calculated apparent diffusion coefficient at different potentials during the charge and discharge processes. (c) Slow scan rate cyclic voltammetry ($5 \mu\text{V s}^{-1}$). T cells, Zinc foils as counter and reference electrodes, 3 m Zn(OTF)_2 aqueous electrolyte.

The variation of the apparent diffusion coefficient with respect to the potential (calculated based on GITT) can be correlated to the SSCV profiles, which demonstrates the mechanism of the observed CV peaks. Since the diffusion coefficient of one material is determined by the guest and the host species, e.g., electronic conductivity of the host material, different intercalation sites, which may vary

depending on the intercalation level, the diffusion coefficient-potential profiles shown in Fig. S10c cannot distinguish which species are intercalated into vanadium oxides.

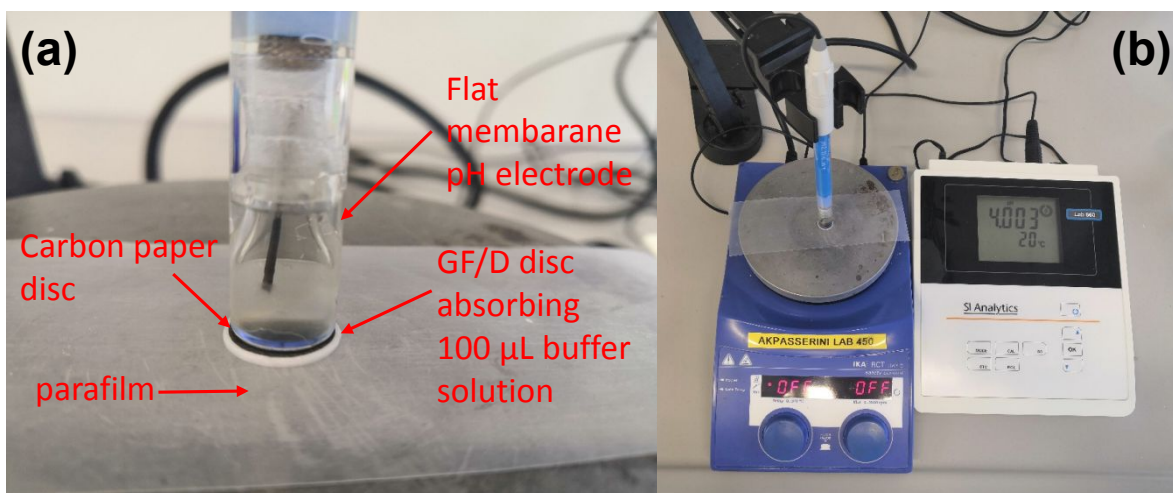


Fig. S11. Images of the set-up used to check the reliability of the flat membrane pH electrode determining the pH of the electrolyte on the surface of a porous carbon paper disc.

A porous carbon paper disc (diameter: 12 mm) was placed on top of a GF/D disc (diameter: 13 mm) impregnated with 100 µL of commercial buffer solution (pH of 4.01 ± 0.01). Then the pH electrode was placed on top of the carbon paper disc to detect the solution's pH. The obtained result, 4.003, demonstrates the good reliability of the system.

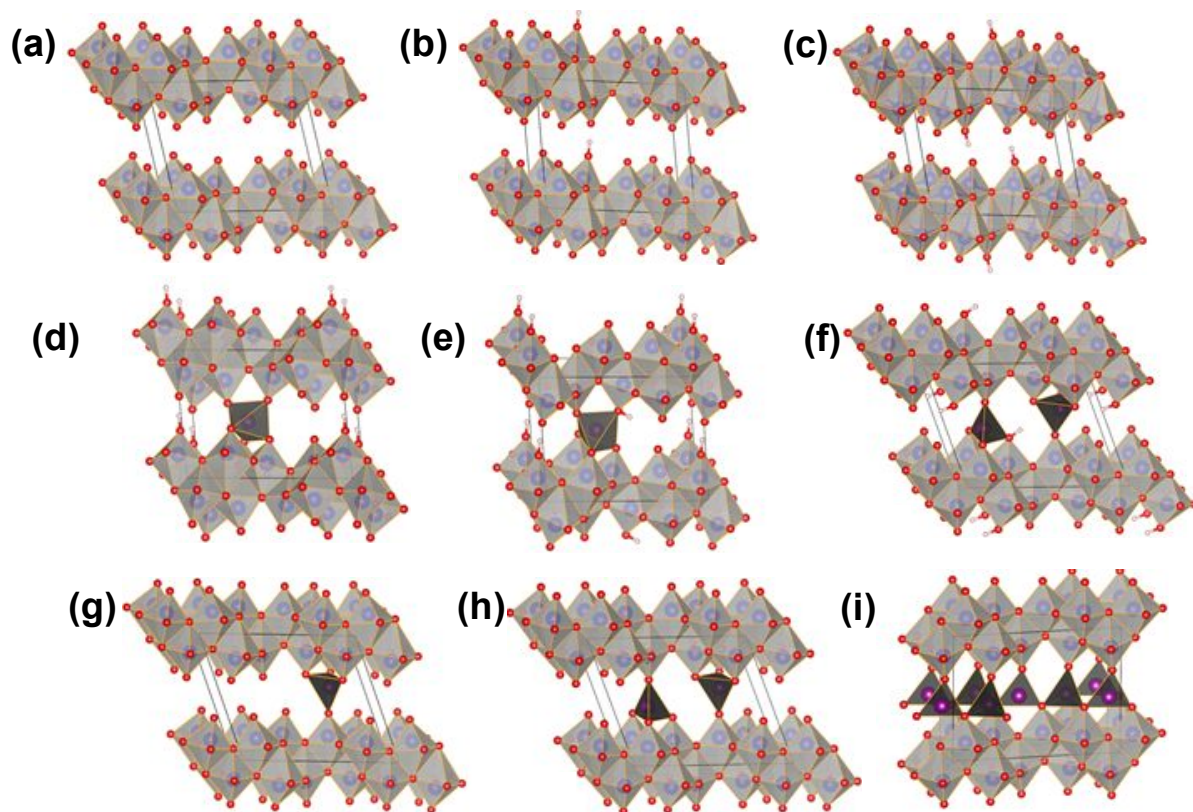


Fig. S12. Energetically most stable structures of δ - V_2O_5 with different H^+ and Zn^{2+} contents: (a) V_2O_5 , (b) $H_{0.25}V_2O_5$, (c) $H_{0.5}V_2O_5$, (d) $H_{0.25}Zn_{0.25}V_2O_5$, (e) $H_{0.5}Zn_{0.25}V_2O_5$, (f) $H_{0.5}Zn_{0.5}V_2O_5$, (g) $Zn_{0.25}V_2O_5$, (h) $Zn_{0.5}V_2O_5$, (i) ZnV_2O_5 .

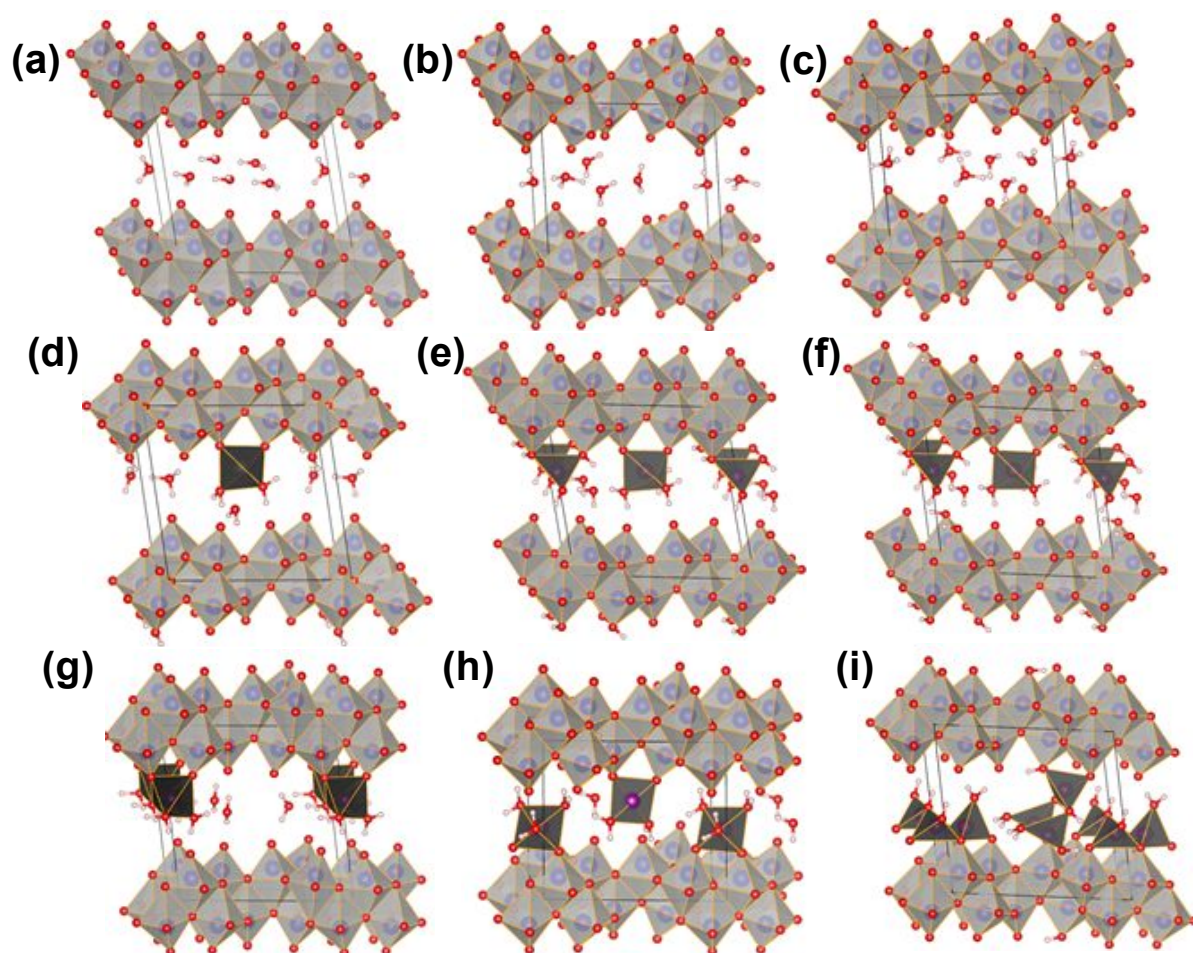


Fig. S13. Energetically most stable structures of δ - $V_2O_5 \cdot H_2O$ with different H^+ and Zn^{2+} contents: (a) $V_2O_5 \cdot H_2O$, (b) $H_{0.25}V_2O_5 \cdot H_2O$, (c) $HV_2O_5 \cdot H_2O$, (d) $H_{0.25}Zn_{0.25}V_2O_5 \cdot H_2O$, (e) $H_{0.25}Zn_{0.5}V_2O_5 \cdot H_2O$, (f) $H_{0.5}Zn_{0.5}V_2O_5 \cdot H_2O$, (g) $Zn_{0.25}V_2O_5 \cdot H_2O$, (h) $Zn_{0.5}V_2O_5 \cdot H_2O$, (i) $ZnV_2O_5 \cdot H_2O$.